

Spatial Normalization of Diffusion Tensor Fields

Dongrong Xu,^{1*} Susumu Mori,² Dinggang Shen,¹ Peter C.M. van Zijl,² and Christos Davatzikos¹

A method for the spatial normalization and reorientation of diffusion tensor (DT) fields is presented. Spatial normalization of tensor fields requires an appropriate reorientation of the tensor on each voxel, in addition to its relocation into the standardized space. This appropriate tensor reorientation is determined from the spatial normalization transformation and from an estimate of the underlying fiber direction. The latter is obtained by treating the principal eigenvectors of the tensor field around each voxel as random samples drawn from the probability distribution that represents the direction of the underlying fiber. This approach was applied to DT images from nine normal volunteers, and the results show a significant improvement in signal-to-noise ratio (SNR) after spatial normalization and averaging of tensor fields across individuals. The statistics of the spatially normalized tensor field, which represents the tensor characteristics of normal individuals, may be useful for quantitatively characterizing individual variations of white matter structures revealed by DT imaging (DTI) and deviations caused by pathology. Simulated experiments using this methodology are also described. Magn Reson Med 50:175–182, 2003. © 2003 Wiley-Liss, Inc.

Key words: diffusion tensor image warping; tensor reorientation; fractional anisotropy; white matter fibers; statistical anatomical atlases

Diffusion tensor imaging (DTI) has emerged during the past several years as a potentially powerful way to map white matter fibers in vivo. DTI takes advantage of the microscopic diffusion of water molecules, which is less restricted along the axis of a fiber than along its transverse direction. DT images are usually acquired by applying at least six noncolinear gradient orientations, and thus measuring a symmetric tensor on each voxel. The principal axis of this tensor presumably coincides with the underlying fiber's orientation. One of the potential applications of this technique is the study of white matter architecture in the brain. In conventional MRI, such as T_1 - and T_2 -weighted images, white matter often appears as a homogeneous structure, even though it consists of many axonal bundles of various sizes and orientations. With the use of fiber orientation information, one can identify various axonal tracts within the homogeneous-looking white matter. This capability of DTI may be useful for studying effects of

development, aging, and diseases on specific white matter tracts of interest.

Despite the promise of this imaging method, the clinical utility of DTI is currently limited by several factors. For instance, even if tracts of interest can be identified visually, proper tools with which to quantify their locations, sizes, and shapes, and to compare them between normal and abnormal populations, are still in their infancy. DTI is also an inherently lengthy imaging technique that produces relatively higher levels of scanner noise. This is particularly a problem in non-cooperative patient populations, since scanning time must be kept to a minimum, which thus decreases noise. Image noise is also detrimental in fiber tractography, since its cumulative effect can cause significant deviations of a pathway tracked along a tensor field from its true position. Similar problems also arise in functional imaging and, particularly, positron emission tomography (PET) as a result of limited SNR. A widely used approach to mitigate the effects of noise in group analysis has been the use of statistical parametric mapping (SPM) (1,2), which usually consists of two steps. First, images from a number of subjects are spatially normalized by a deformable registration procedure, which accounts for interindividual morphological variability, and maps image data to a canonical (stereotaxic) space. A subsequent statistical analysis is used to identify consistent trends across subjects, from noisy image measurements. A simple way to describe this approach is to say that it increases SNR by averaging across subjects. The probability map generated from this procedure is called a "statistical atlas." A statistical map of anatomy reflects the probability of finding a particular structure at a given location, within a group of individuals.

Our premise in this work is that by jointly examining DT images from many individuals, one can statistically characterize the complex white matter architecture and better detect abnormalities in brain connectivity.

It is more complicated to apply spatial normalization to tensor fields than to scalar images (3,4). This is because the tensor must be reoriented on each image voxel, in addition to a voxel displacement that is implied by the spatial normalization transformation. This is achieved by finding the rotational component of the spatial normalization transformation. Moreover, this rotation depends on the actual orientation of the underlying fiber, which is not known a priori. In this study we solve this problem by adopting a statistically based reorientation strategy, which is based on estimating the probability density function (PDF) of the underlying fiber, based on the tensor measurements, and using it along with the Procrustes fit to estimate the appropriate rotational component that reorients the tensor measurements. We apply this procedure in conjunction with a very-high-dimensional elastic registration method (5) on images from nine normal volunteers, and

¹Section of Biomedical Image Analysis, Department of Radiology, University of Pennsylvania School of Medicine, Philadelphia, Pennsylvania.

²F.M. Kirby Research Center for Functional Brain Imaging, Johns Hopkins University School of Medicine, Baltimore, Maryland.

Grant sponsor: NIH; Grant numbers: NIH-AG-93-07; R01-AG014971; R01-AG20012-01; P41-RR15241-01A1.

*Correspondence to: Dongrong Xu, 3600 Market St., Suite 380, Philadelphia, PA 19104. E-mail: xdr@rad.upenn.edu

Received 20 March 2002; revised 19 February 2003; accepted 21 February 2003.

DOI 10.1002/mrm.10489

Published online in Wiley InterScience (www.interscience.wiley.com).

© 2003 Wiley-Liss, Inc.

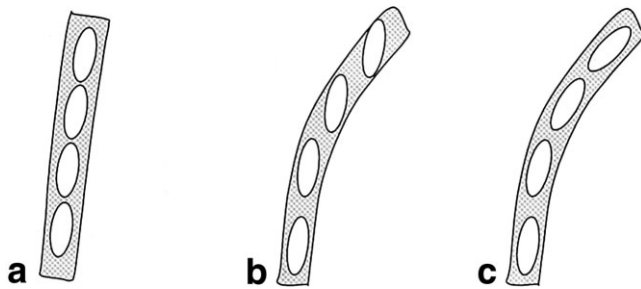


FIG. 1. Tensors must be reoriented in addition to being relocated during DTI warping. **a**: Original tensor field. **b**: Warped tensor field without tensor reorientation (this result would be obtained if, for example, each tensor was warped as a scalar image voxel). **c**: Warped tensor field with tensor properly reoriented.

we demonstrate that it significantly reduces noise and thus highlights major fiber pathways.

METHODS

Image Warping (Spatial Normalization)

Image warping for deformable registration has received a great deal of attention during the past decade (e.g., Refs. 2,6–13). In the present work we used a very-high-dimensional elastic transformation procedure in 3D volume space, referred to as the “hierarchical attribute matching mechanism for elastic registration” (HAMMER) method, which is determined from T_1 -weighted images and applied on coregistered DT images. This approach uses image attributes to determine point correspondences between an individual image and a template, which resides in the stereotaxic space and is used as the target to which all individual images are warped. A hierarchical sequence of piece-wise smooth transformations is then determined, so that the attributes of the warped images are as similar as possible to the attributes of the target. Relatively fewer, more stable attributes are used in the initial stages of this procedure, which helps avoid local minima, a known problem in high-dimensional transformations. The details of this algorithm can be found in Ref. 5.

Ideally, even if the spatial normalization method were able to remove most of the variability in gray matter anatomy, residual variability in the white matter anatomy would still exist, because of variability in fiber thickness and orientation. Our goal is to develop ways to measure this variability, and to use this normative data to quantify effects of pathological processes affecting brain connectivity.

Tensor Reorientation

It is a simple matter to warp a scalar image by a known spatial transformation. The image value from a particular voxel is transferred, via the displacement field of the spatial transformation, to a voxel in the target image. Typically, some sort of interpolation must also be applied. However, a more complex procedure is required to warp tensor fields. Suppose there is a fiber bundle as shown in Fig. 1a. It would be erroneous to simply carry the tensor values to the target voxel, as shown in Fig. 1b, as one

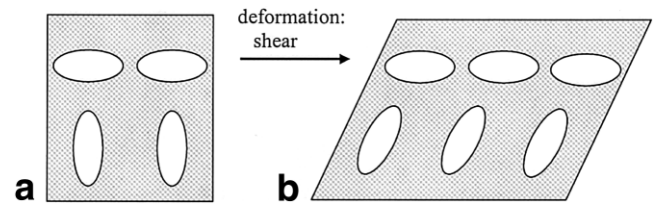


FIG. 2. The tensor’s orientation in relation to the deformation direction is important in tensor reorientation. **a**: Original tissue. **b**: Deformed tissue. The tensors on the top row are unchanged, whereas the tensors on the bottom row are reoriented, despite the fact that the spatial transformation is constant throughout the rectangle. This reveals the dependency of the tensor reorientation on the orientation of the fiber relative to the spatial transformation.

would do for scalar images. The tensor must be reoriented appropriately, as shown in Fig. 1c. One could estimate the rotational component of the warping transformation around each voxel, and use that to reorient the tensor measurements. However, this would also be wrong, since the appropriate rotation angles depend on the underlying fiber’s orientation. This can be puzzling, at first, but it is explained schematically in Fig. 2. In Fig. 2a, we show a hypothetical shape, along with the respective tensor measurements, which is transformed to that of Fig. 2b via a simple linear transformation. Although the spatial transformation is the same on all voxels, the voxels at the top receive no rotation, since the tensors are oriented in parallel to the direction of shearing. However, the bottom two tensors are rotated appropriately. This implies that exactly the same warping transformation should have different rotation effects on differently oriented tensors.

Moreover, the tensor’s shape must be preserved when the DT fields are warped. Suppose the local transformation is a horizontal stretching (scaling), as shown in Fig. 3a. If this transformation is used to transform the tensor field as

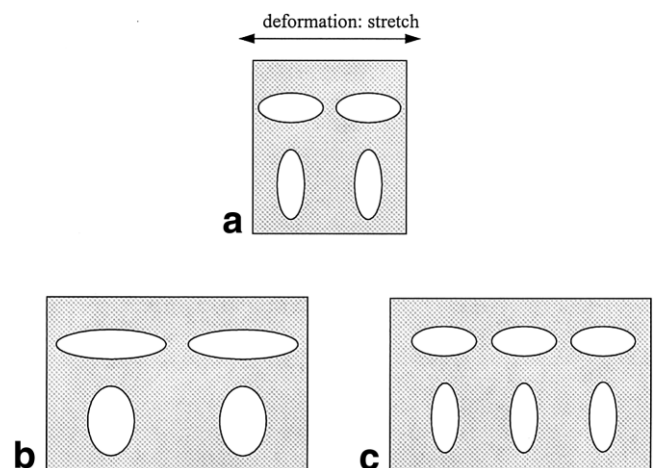


FIG. 3. The tensor’s shape must be preserved during elastic deformation of DT images, in order for the tensors to correctly reflect the local diffusion property. **a**: Original tissue. **b**: Wrong result if the spatial warping transformation is directly used. **c**: Correctly deformed DT field, which maintains the original tensor measurements during spatial normalization.

in Fig. 3b, the tensor's shape will be deformed. Since the tensor's shape reflects the tissue's local microstructure, which does not change, this result is wrong. The correct result is shown in Fig. 3c, where the tensor's shape remains the same, and only the number of tensors along the local deformation direction is increased to show the stretching effect.

Ideally, if we know the direction, \mathbf{v} , of the fiber on voxel with coordinates \mathbf{x} , we can readily find the rotated version, \mathbf{v}' , of \mathbf{v} , according to the warping transformation. If \mathbf{U} is the matrix that rotates \mathbf{v} to \mathbf{v}' , then \mathbf{U} should be applied to the respective tensor measurement. However, in practice we do not know \mathbf{v} . In fact, this is precisely what we would like to estimate. We only have a noisy orientation of \mathbf{v} , which is the principal direction (PD) of the corresponding tensor measurement. One could use that PD in place of \mathbf{v} , as proposed in Ref. 4. However, that makes the approach vulnerable to noise, since the PD is only a noisy observation, and could be quite different from the true underlying fiber orientation.

Assuming that we know the PDF, $f(\mathbf{v})$, of the fiber direction \mathbf{v} , we can find the rotation matrix, $\tilde{\mathbf{U}}$ which minimizes the expected value of $\|\mathbf{v}' - \mathbf{U}\mathbf{v}\|^2$ over all orthonormal matrices \mathbf{U} :

$$\begin{aligned} \tilde{\mathbf{U}} &= \underset{\mathbf{U}}{\operatorname{argmin}} E\{\|\mathbf{v}' - \mathbf{U}\mathbf{v}\|^2\} \\ &= \underset{\mathbf{U}}{\operatorname{argmin}} \int p d f(\mathbf{v}) \|\mathbf{v}' - \mathbf{U}\mathbf{v}\|^2 d\mathbf{v}. \end{aligned}$$

This problem can be solved by the Procrustean estimation (14), if a number of random samples, \mathbf{v} , are drawn from the PDF, and their respective rotated versions, \mathbf{v}' , are found by the rotation that the warping field applies to \mathbf{v} . If we arrange these vectors \mathbf{v}' and \mathbf{v} to form the columns of the matrices \mathbf{A} and \mathbf{B} , respectively, then $\tilde{\mathbf{U}}$ is found by minimizing:

$$\|\mathbf{A} - \mathbf{U} \cdot \mathbf{B}\|_2^2 = \|\mathbf{A}\|_2^2 + \|\mathbf{B}\|_2^2 + 2 \sum_i \omega_i (\mathbf{A} \cdot \mathbf{B}^T)$$

where $\omega_i(\mathbf{M})$ is the singular value of matrix \mathbf{M} . Via SVD decomposition of $\mathbf{A} \cdot \mathbf{B}^T$, $\tilde{\mathbf{U}}$ can be determined:

$$\begin{aligned} \tilde{\mathbf{U}} &= \mathbf{V} \cdot \mathbf{W}^T \\ \mathbf{A} \cdot \mathbf{B}^T &= \mathbf{V} \cdot \mathbf{\Omega} \cdot \mathbf{W}^T \end{aligned}$$

Estimating the PDF $f(\cdot)$

In the above derivations, we assume that the PDF $f(\cdot)$ of the fiber's orientation is known. However, in practice this is not the case. To overcome this limitation, we use the tensor measurements in a small neighborhood, $N(\mathbf{x})$, around voxel \mathbf{x} , to obtain observations of the random variable \mathbf{v} . Our assumption is that if $N(\mathbf{x})$ is of the appropriate shape and size, the fiber's orientation, and therefore $f(\cdot)$, remains approximately constant within $N(\mathbf{x})$. Accordingly, the PDs of the tensor measurements within $N(\mathbf{x})$ are used

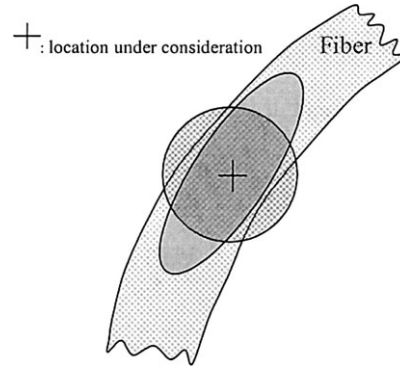


FIG. 4. The ellipsoid and the sphere have the same volume, but the former has been appropriately shaped based on the fiber's orientation.

as random samples drawn from $f(\cdot)$. These samples are then used to form the matrices \mathbf{A} and \mathbf{B} described above, and to estimate $\tilde{\mathbf{U}}$ via the Procrustean estimation procedure.

The neighborhood $N(\mathbf{x})$ must be of the appropriate shape to avoid including tensor measurements from nonoriented tissue adjacent to the fiber. This is shown schematically in Fig. 4, which indicates that $N(\mathbf{x})$ should be elongated, rather than spherical. Accordingly, we estimate $N(\mathbf{x})$ via the following iterative procedure: First, select the volume, V , of $N(\mathbf{x})$, and start with a spherical neighborhood. Then calculate the average tensor within $N(\mathbf{x})$, and reshape $N(\mathbf{x})$ to have the same orientation and axes ratio, while maintaining the volume V constant. Then iterate this procedure until convergence. Theoretically, keeping V fixed ensures that the total number of random samples \mathbf{v} drawn from within $N(\mathbf{x})$ is the same for all voxels, and hence the degree of smoothing applied in this estimation procedure is uniform throughout the image. In practice, when the resolution of the DT volume is nonisotropic, we need to resample the DT volume and make it isotropic, so that the volume of neighborhood can be kept constant.

Our algorithm for estimating $\tilde{\mathbf{U}}$ is summarized as follows:

- Step 1. Find the neighborhood $N(\mathbf{x})$, according to the iterative procedure described above.
- Step 2. Find the PD of the tensor measurements on all voxels included in $N(\mathbf{x})$, and their respective rotated versions by the warping transformation.
- Step 3. Use the vectors of step 2 to form matrices \mathbf{A} and \mathbf{B} , and use the singular value decomposition procedure to estimate the rotation (orthonormal) matrix $\tilde{\mathbf{U}}$ that minimizes $(\|\mathbf{A} - \mathbf{U}\mathbf{B}\|_2)^2$.
- Step 4. Apply $\tilde{\mathbf{U}}$ to reorient the tensor on voxel \mathbf{x} . The tensor is also repositioned, according to the warping transformation, which effectively places the tensor in its canonical coordinates in the stereotaxic space and in the appropriate orientation.

This procedure reorients the tensor based only on the tensor's principal direction, and may not necessarily rotate its second PD properly. The process must be repeated for

the second PD as well. However, the reorientation of the second PD can only be implemented under the premise that the three PDs span an orthogonal space. Therefore, for the second PDs in steps 1 and 2, we use the projection of their original and rotated versions on a plane that is perpendicular to the reoriented first PD, i.e., $\tilde{\mathbf{U}}_1 \cdot \mathbf{PD}_1$, where \mathbf{PD}_1 is the tensor's first PD and $\tilde{\mathbf{U}}_1$ is the corresponding reorientation matrix. If we obtain $\tilde{\mathbf{U}}_2$ as the reorientation matrix for the tensor's second PD, we may reorient the tensor \mathbf{D} as follows:

$$\mathbf{D}_{rotated} = \tilde{\mathbf{U}}_2 \cdot \tilde{\mathbf{U}}_1 \cdot \mathbf{D} \cdot \tilde{\mathbf{U}}_1^T \cdot \tilde{\mathbf{U}}_2^T.$$

Suppose

$$D = \Pi \cdot \Lambda \cdot \Pi^T,$$

where

$$\Pi = (\tilde{\mathbf{v}}_1 \tilde{\mathbf{v}}_2 \tilde{\mathbf{v}}_3), \Lambda = \begin{pmatrix} \lambda_1 & & \\ & \lambda_2 & \\ & & \lambda_3 \end{pmatrix}.$$

Because $\tilde{\mathbf{U}}_2$ rotates along axis $\tilde{\mathbf{U}}_1 \cdot \mathbf{PD}_1$,

$$\mathbf{D}_{rotated} = (\tilde{\mathbf{U}}_1 \cdot \tilde{\mathbf{v}}_1 \tilde{\mathbf{U}}_2 \cdot \tilde{\mathbf{U}}_1 \cdot \tilde{\mathbf{v}}_2 \tilde{\mathbf{U}}_2 \cdot \tilde{\mathbf{U}}_1 \cdot \tilde{\mathbf{v}}_3) \cdot \Lambda \cdot (\tilde{\mathbf{U}}_1 \cdot \tilde{\mathbf{v}}_1 \tilde{\mathbf{U}}_2 \cdot \tilde{\mathbf{U}}_1 \cdot \tilde{\mathbf{v}}_2 \tilde{\mathbf{U}}_2 \cdot \tilde{\mathbf{U}}_1 \cdot \tilde{\mathbf{v}}_3)^T.$$

Thus, both the tensor's first and second PDs, and consequently the third, are appropriately rotated, and $\tilde{\mathbf{U}} = \tilde{\mathbf{U}}_2 \cdot \tilde{\mathbf{U}}_1$ is the tensor reorientation matrix that we are trying to find. A similar consideration was discussed in Ref. 4; however, in that study the rotated \mathbf{PD}_2 was projected, whereas we project \mathbf{PD}_2 before it has been rotated.

DTI Data Acquisition

Our experiments were performed using 1.5 T Philips Gyroscan NT. For the diffusion-weighted imaging (DWI), multislice (coronal) segmented spin-echo EPI with diffusion weighting was used. The imaging dimension was 128×70 for a rectangular field of view (FOV = 250×137 mm). At each scan, 17 echoes were acquired (four-shot EPI) with one navigator echo for phase correction (bandwidth/pixel = 1679.7 (readout) and 66.4 (phase encode) Hz). Fourier coverage in the phase-encode direction was 97%. In-plane zero-filling to 256×140 was used. The slice thickness was 3.0 mm without a gap, and 50–60 slices covered the entire brain, from which 3D volume DTI data were reconstructed. Because of the short echo train length, b_0 -related image deformation was minimal (16,17). For anatomical information, 3D T_1 -weighted images (spoiled gradient-echo (SPGR), flip angle = 30° , TR = 21 ms, and TE = 4.6 ms, bandwidth/pixel = 359.4 Hz) were also acquired using an FOV of 250 mm. The imaging matrix size was 128×128 , which was zero-filled to 256×256 .

The data from diffusion-weighted (DW) images along six independent axes and the least DW image were combined to calculate the six independent variables in the DT (15). The tensor matrix in each voxel was subsequently diagonalized to obtain the three eigenvalues and eigenvectors.

In this study we used T_1 -weighted images for anatomical normalization. In this process, it is very important that the EPI-based DTI images are well coregistered with minimum b_0 -related distortion. The segmented EPI with 17 echoes used in this study fulfilled this condition, as shown in Fig. 5, in which the contour of the brain defined by the segmented EPI was superimposed on T_1 -weighted images. We can see that mismatching occurs only in a few small regions around the sinus. DW images with six noncolinear orientations and one least-weighted image were collected within 5–8 min. The scanning was repeated six times to improve the SNR. Coregistered with each DT image was a standard T_1 -weighted image obtained during the same session. The coregistration was realized by the UCLA-AIR program (18,19).

Experiments

We performed two experiments. In our first experiment, we collected data from nine normal volunteers. The data resolution was $0.977 \times 0.977 \times 3.00$ mm. After the DT and SPGR images were collected and coregistered, we applied our warping and reorientation procedure to spatially normalize eight tensor images, by treating the ninth image as the target. We calculated the average tensor field of the nine subjects, by voxel-wise averaging the corresponding components of the corresponding tensors of these spatially normalized and reoriented tensor images. The purpose of this experiment was to demonstrate that DT image SNR can be significantly improved after the images from a number of subjects have been pooled and properly registered.

In our second experiment, we simulated a hypothetical abnormality that affects the tensor measurements. Our goal was to use the data from the nine normal subjects to form a statistical atlas of normal DT properties in a standardized space, and to use this atlas to identify regions that displayed significantly different fractional anisotropy (FA) (20) in the image with the simulated abnormality. We randomly picked one normal case from the nine subjects, and modified the tensor shape at certain regions on a main fiber pathway by adding atrophy, which effectively made the respective tensors rounder (less elongated) and the FA values smaller. Let \mathbf{D} be a tensor, with eigenvalues $\lambda_1, \lambda_2, \lambda_3$, and eigenvectors $\mathbf{v}_1, \mathbf{v}_2, \mathbf{v}_3$. For a degradation percentage x , we simulate the abnormality as follows:

Step 1. Let $\lambda := \max \{\lambda_1, \lambda_2, \lambda_3\}$

Step 2. Set $\lambda_1 := \lambda_1 + (\lambda - \lambda_1) \times x$

Step 3. Set $\mathbf{D} := (\mathbf{v}_1 \mathbf{v}_2 \mathbf{v}_3) \cdot \begin{pmatrix} \lambda_1 & 0 & 0 \\ 0 & \lambda_2 & 0 \\ 0 & 0 & \lambda_3 \end{pmatrix} \cdot (\mathbf{v}_1 \mathbf{v}_2 \mathbf{v}_3)^T$

Obviously, 100% degradation will create a sphere, the fractional anisotropy of which is 0.

We used different values for x —10%, 20%, 30%, and 40%—with percentage changes in the FA values of about 8.41%, 16.75%, 24.88%, and 32.75%, respectively. To make the edge of the simulated abnormality merge naturally into the normal region, we gradually decreased the degradation percentage beyond the region of simulated atrophy and within a larger spherical region.

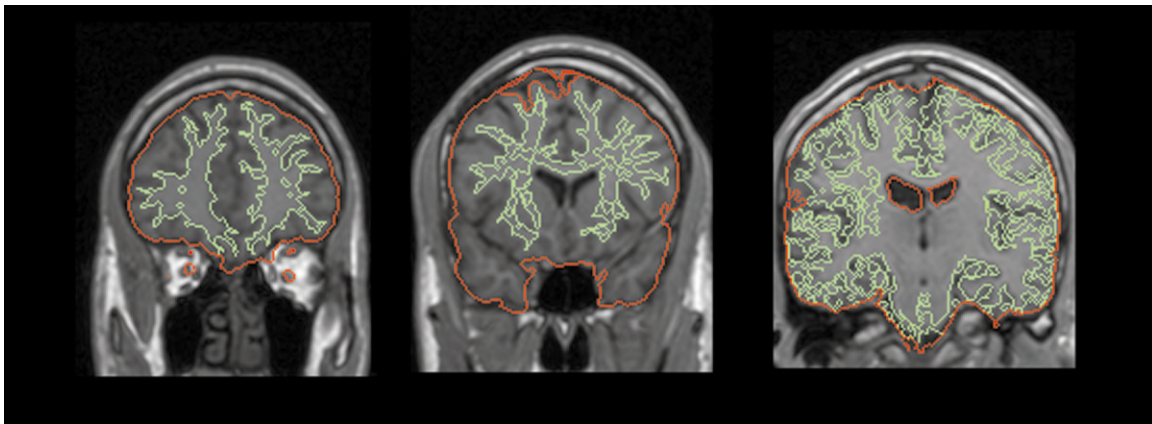


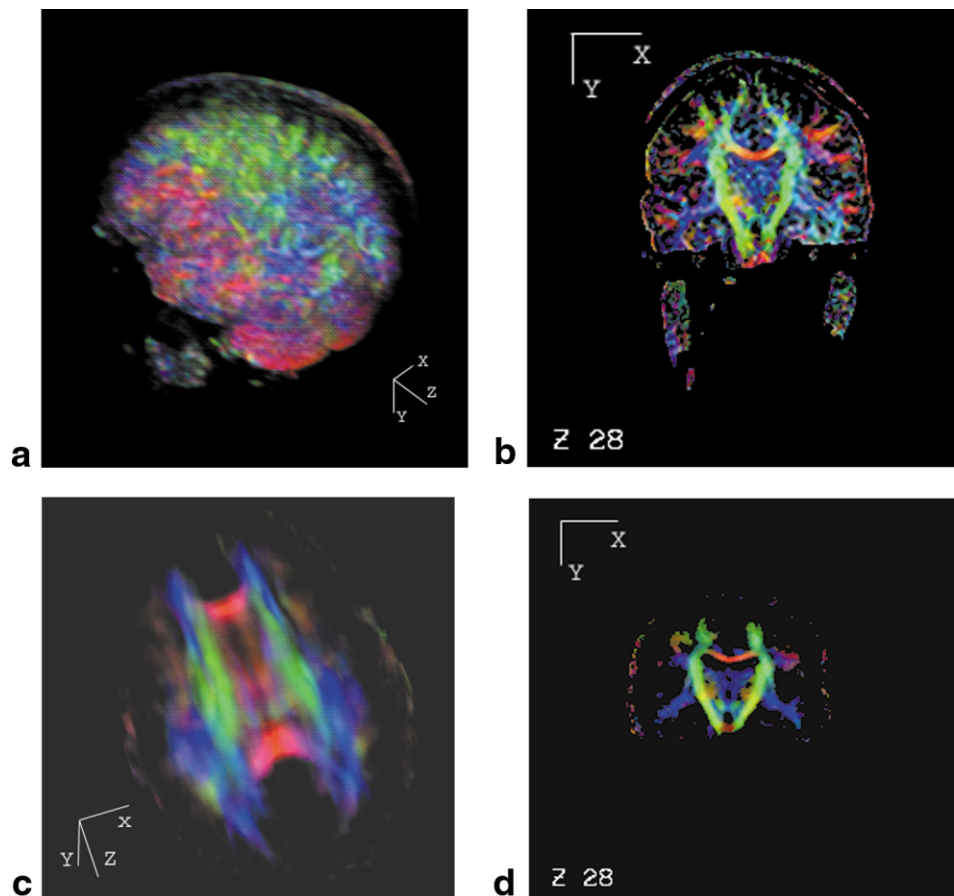
FIG. 5. Image distortion in DT images. The boundaries of the brain (red line) and the white matter (green line) were defined in anisotropy maps and superimposed on SPGR (T_1 -weighted) images at the same slice levels. A slight mismatch can be seen in only a few small regions around the sinus. The anisotropy maps were obtained from a four-segmented EPI sequence.

RESULTS

Nine normal subjects (male and female, of different ages) were randomly selected from our database. We used one of the nine as a template and registered to it the remaining eight brains. Figure 6a and b shows a 3D rendering and a typical cross-section of the color-coded PD of one of the individual tensor fields; Fig. 6c and d shows those of the average tensor field of the nine normal volunteers. The PD

of the tensor fields was multiplied by the FA value, and color-coded as customary. Red was assigned to the x -component, green to the y -component, and blue to the z -component. For clarity, the resulting PD fields were thresholded at $FA = 0.2$, so only tissue that displays significant anisotropy is shown. We can see that after the registration and averaging procedure, noise was removed, and the main fiber bundles became visible.

FIG. 6. Color map of the primary direction of one individual's DT image in original individual space, and of the average tensor field of nine subjects after spatial normalization and tensor reorientation, where the x -component is mapped to red, y to green, and z to blue. **a:** A 3D-rendered view of one individual DT image. **b:** A typical coronal slice of the same individual brain. A significant amount of noise is apparent. **c:** 3D view of the average DT field. **d:** A representative coronal slice of the same average tensor field.



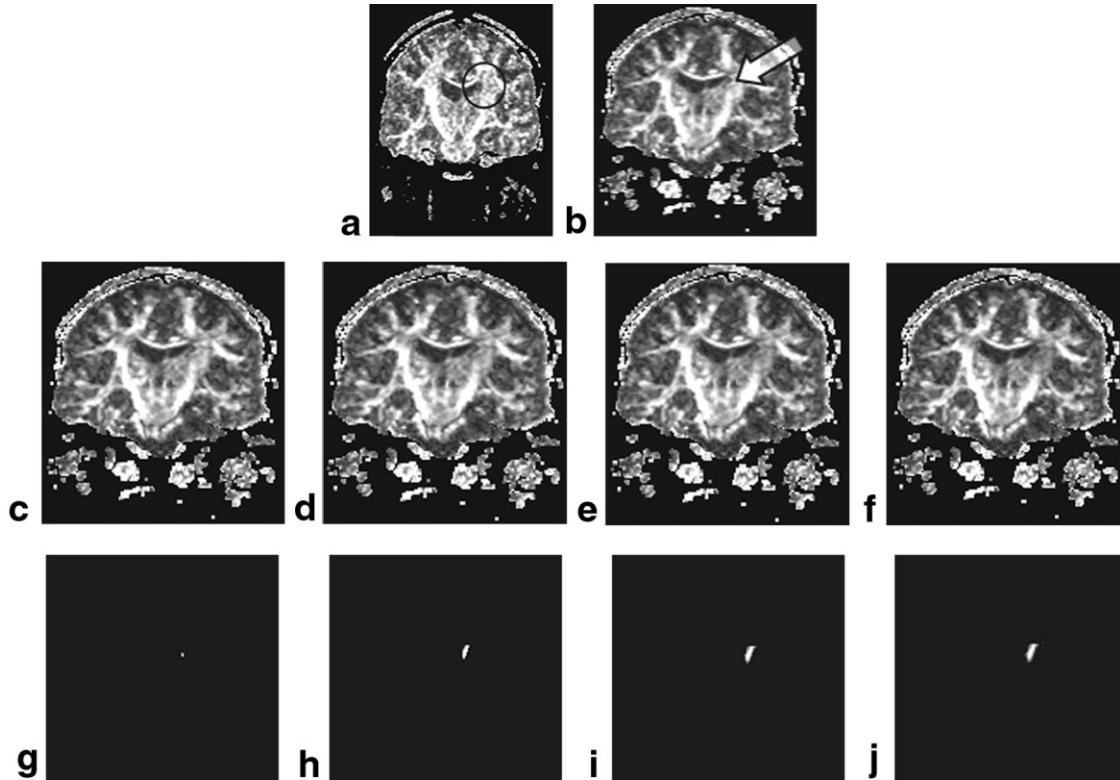


FIG. 7. Result of the second experiment. **a**: A typical slice of the FA volume of the normal brain before warping. The circle indicates the area for different levels of simulated abnormality to be added. **b–f**: The corresponding slices of the FA volumes of the warped individual tensor field with different atrophy simulations. **b**: The corresponding slice of the FA map of the warped tensor field without any abnormality ($x = 0$), where the arrow indicates the simulation area. **c**: $x = 10\%$. **d**: $x = 20\%$. **e**: $x = 30\%$. **f**: $x = 40\%$. **g–j**: Detected abnormalities in common structure areas, corresponding to different degradation percentages of 10–40%, respectively (voxels with z-scores higher than the maximum z-score observed in the nine training images from which the statistical atlas was constructed).

Since we performed voxel-wise statistics to determine abnormal voxels, we smoothed all the FA volumes calculated from the nine images with a Gaussian filter of 5-mm standard deviation, so that noise (and hence the voxel-wise variance of tensor FA) is decreased. We then averaged these nine smoothed volumes and obtained an average FA volume, which highlighted the common fiber structures in white matter. These common structure areas formed a mask for our second experiment, in which we sought to locate any potential abnormalities, such as FA deviation or fiber disruption.

Figure 7a displays the FA of the normal brain for abnormality-simulation in this individual's original space before warping. A circle indicates the region where simulated atrophy was to be added with different values of x . Figure 7b–f shows the FA of the warped versions of the brain with different simulated abnormality levels. The arrow in Fig. 7b points to the location in the warped normal brain where the simulated abnormality is to be found in Fig. 7c–f. To detect the abnormality through use of a comparison with the atlas, we calculated the z-score for every voxel in the smoothed version of the normalized image with simulated atrophy, and we thresholded it according to the maximum z-score (whose absolute value is 2.41 in our case) of the smoothed FA maps of the normal individuals' warped DT images. Voxels with higher z-scores were

labeled as abnormal. Figure 7g–j shows the detected abnormalities, for different levels of x from 10% to 40%. Figure 8 depicts the 3D-volume-rendered views of the detected abnormalities displayed in the normalized individual brain space.

DISCUSSION

We have presented a methodology for the spatial normalization and reorientation of DT fields. Estimating the appropriate reorientation strategy is not straightforward, since it depends on knowledge of the underlying fiber direction. Since such knowledge is not available in practice, we adopted a statistical formulation in which the orientation of the underlying fiber on every voxel is assumed to follow a probability distribution, which is estimated from measurements around that voxel. The rotation matrix that reorients the tensor at that voxel is then estimated via the Procrustean fit, which effectively finds the single rotation matrix that best fits the reorientation implied by the warping field along the direction of random samples from the probability distribution of the fiber direction.

We applied this procedure to data from nine normal volunteers, by spatially normalizing their DT images using spatial transformations that were determined from core-

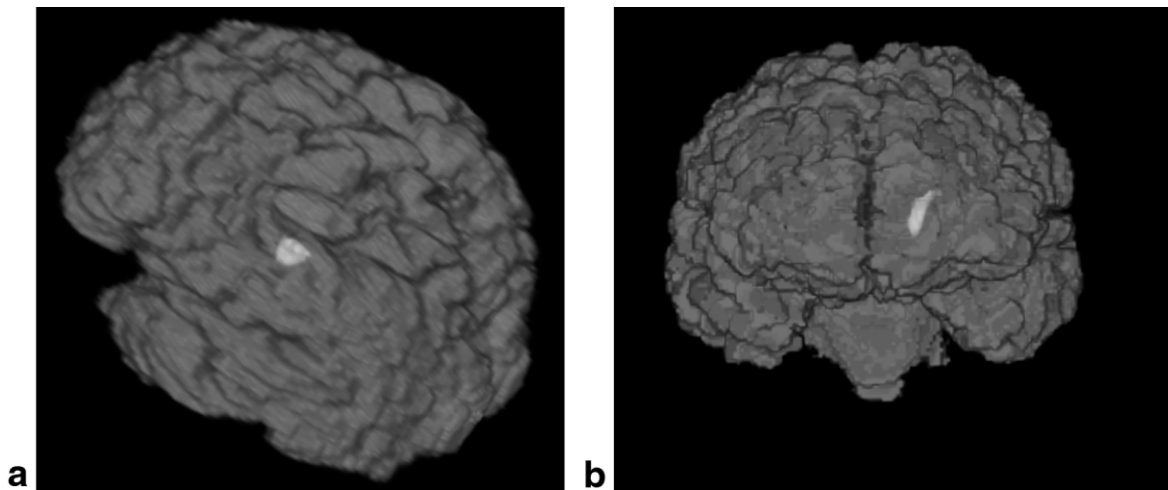


FIG. 8. Detected abnormalities (green) embedded in the individual's warped 3D brain image. **a:** Lateral view. **b:** Frontal view. [Color figure can be viewed in the online issue, which is available at www.interscience.wiley.com.]

istered T_1 -weighted images. Spatial normalization allows us to then average data from multiple subjects, thereby dramatically reducing the level of noise in the tensor measurements. This could ultimately help overcome some of the current limitations of fiber-tracking methods, particularly limitations related to the high levels of noise in DTI data. However, it is important to note that tracking fibers on the average of spatially normalized tensor fields can only help us reconstruct common aspects of fiber anatomy, and not individual deviations.

Our goal is to use this methodology to determine a voxel-wise statistical representation of the DT properties in normal populations. This representation can then be used as normative data to identify particular fibers that are affected by disease. For example, the general linear model (2,17) can be expanded to apply to tensor data, thereby allowing the performance of voxel-wise statistical tests on the spatially normalized tensor fields to identify group differences or correlations between changes in white matter fibers and clinical data. Potential applications include the study of abnormalities in development, aging, and psychiatric disorders in which abnormalities in specific white matter tracts are suspected.

In this work, we averaged the tensors component-wise at corresponding voxels of the nine subjects. However, if the six DW directions of the raw scalar images could be managed to rotate with each pixel and be memorized, the consequent reconstruction of a warped DT field would be feasible. Nevertheless, this is only a different means of reorienting the DT field, and will provide the same result as we offer through our approach, which is more straightforward.

Distortion in the EPI sequence could present a problem, in that it causes disagreement between the DT image and the T_1 -weighted image from which the spatial normalization is determined. Our data sets show that this was a minor problem in our experiments, as demonstrated in Fig. 5. However, if the coregistration of the T_1 -weighted and DT images is poor, a potential solution would be to use the b_0 image to find the spatial normalization transfor-

mation directly, rather than using a coregistered T_1 -weighted image. The b_0 images are perfectly coregistered with the tensor field; however, the b_0 images (which usually are heavily T_2 -weighted) may not have optimal gray and white matter contrast, which could reduce the accuracy of the spatial normalization. Studies addressing this issue are under way in our laboratory.

REFERENCES

1. Friston KJ, Ashburner J, Frith CD, Poline JB, Heather JD, Frackowiak RSJ. Spatial registration and normalization of images. *Hum Brain Mapp* 1999;2:165–189.
2. Friston KJ, Holmes AP, Worsley KJ, Poline JP, Frith CD, Frackowiak RSJ. Statistical parametric maps in functional imaging: a general linear approach. *Hum Brain Mapp* 1995;189–210.
3. Alexander DC, Gee JC, Bajcsy R. Strategies for data reorientation during non-rigid warps of diffusion tensor images. In: *Proceedings of MICCAI, the Second International Conference*, Cambridge, UK, 1999. p 463–472.
4. Alexander DC, Pierpaoli C, Basser PJ, Gee JC. Spatial transformations of diffusion tensor magnetic resonance images. *IEEE Trans Med Imaging* 2001;20:1131–1139.
5. Shen D, Davatzikos C. HAMMER: hierarchical attribute matching mechanism for elastic registration. *IEEE Trans Med Imaging* 2002;21:1421–1439.
6. Collins DL, Neelin P, Peters TM, Evans AC. Automatic 3D intersubject registration of MR volumetric data in standardized Talairach space. *J Comp Assist Tomogr* 1994;18:192–205.
7. Davatzikos C, Bryan RN. Using a deformable surface model to obtain a shape representation of the cortex. *IEEE Trans Med Imaging* 1996;15:785–795.
8. Davatzikos C. Mapping of image data to stereotaxic spaces: applications to brain mapping. *Hum Brain Mapp* 1998;6:334–338.
9. Davatzikos C, Genc A, Xu D, Resnick SM. Voxel-based morphometry using the RAVENS maps: methods and validation using simulated longitudinal atrophy. *Neuroimage* 2001;14:1361–1369.
10. Gee JC, Reivich M, Bajcsy R. Elastically deforming 3D atlas to match anatomical brain images. *J Comput Assist Tomogr* 1993;17:225–236.
11. Thompson P, Toga AW. A surface-based technique for warping three-dimensional images of the brain. *IEEE Trans Med Imaging* 1996;15:402–417.
12. Vaillant M, Davatzikos C. Hierarchical matching of cortical features for deformable brain image registration. In: *Lecture Notes in Computer Science: Information Processing in Medical Imaging* 1999;1613:182–195.

13. Christensen GE, Rabbitt RD, Miller MI. 3D brain mapping using a deformable neuroanatomy. *Phys Med Biol* 1994;39:609–618.
14. Golub GH, Van Loan CF. *Matrix computations*. Baltimore: Johns Hopkins University Press; 1983.
15. Pierpaoli C, Basser PJ. Toward a quantitative assessment of diffusion anisotropy. *Magn Reson Med* 1996;36:893–906.
16. Mori S, Kaufmann WE, Davatzikos C, Stieltjes B, Amodei L, Fredericksen K, Pearlson GD, Melhem ER, Solaiyappan M, Raymond GV, Moser HW, van Zijl PCM. Imaging cortical association tracts in human brain using diffusion tensor-based axonal tracking. *Magn Reson Med* 2002;47:215–223.
17. Stieltjes B, Kaufmann WE, van Zijl PCM, Fredericksen K, Pearlson GD, Mori S. Diffusion tensor imaging and axonal tracking in the human brainstem. *NeuroImage* 2001;14:723–735.
18. Woods RP, Grafton ST, Holmes CJ, Cherry SR, Mazziotta JC. Automated image registration. I. General methods and intra-subject, intra-modality validation. *J Comput Assist Tomogr* 1998;22:141–154.
19. Woods RP, Grafton ST, Watson JDG, Scotte NL, Mazziotta JC. Automated image registration. II. Inter-subject validation of linear and non-linear models. *J Comput Assist Tomogr* 1998;22:155–165.
20. Pierpaoli C, Jezzard P, Basser PJ, Barnett A, Di Chiro G. Diffusion tensor MR imaging of human brain. *Radiology* 1996;201:637–648.